26 May 2010, 5:30 pm - 6:00 pm

Zero-Gravity Triaxial Shear Tests on Mechanical Properties of Liquefied Sand and Performance Assessment of Mitigations Against Large Ground Deformation

Ikuo Towhata
University of Tokyo, Japan

Trinh Thi Lan Anh
Electricity of Vietnam, Vietnam

Suguru Yamada
University of Tokyo, Japan

Ramin Motamed
ARUP Geotechnics, U.K.

Yoshikazu Kobayashi
Nihon University, Japan


Fifth International Conference on
Recent Advances in Geotechnical Earthquake Engineering and Soil Dynamics
and Symposium in Honor of Professor I.M. Idriss
May 24-29, 2010 • San Diego, California

ZERO-GRAVITY TRIAXIAL SHEAR TESTS ON MECHANICAL PROPERTIES OF LIQUEFIED SAND AND PERFORMANCE ASSESSMENT OF MITIGATIONS AGAINST LARGE GROUND DEFORMATION

Ikuo Towhata
University of Tokyo
Tokyo, JAPAN 113-8656

Trinh Thi Lan Anh
Electricity of Vietnam
VIETNAM

Suguru Yamada
University of Tokyo
Tokyo, JAPAN 113-8656

Ramin Motamed
ARUP Geotechnics
London, UK

Yoshikazu Kobayashi
Nihon University
Tokyo, JAPAN 101-8308

ABSTRACT

This paper concerns prediction of liquefaction-induced large deformation of geotechnical structures that will play major roles in practice of seismic performance design. To do this prediction, it is essential to establish a mechanical model for liquefied sand in which effective stress is null or extremely low. Although past model tests suggested that liquefied sand behaves similar to viscous liquid, there is an opinion against it that pore water pressure distribution in embedded structures produces an apparent rate-dependent behavior. This opinion was examined precisely and quantitatively by analyzing a full-scale model test to find that the pore pressure theory cannot account for the observed behavior. Then the authors conducted a new type of triaxial tests in which the effective stress was made extremely low, similar to the situation in fully liquefied sand, by free falling of a test device in a vertical shaft, thus making the gravity be zero, and a rate-dependent nature of liquefied sand was observed. By using the observed behavior of liquefied sand, a viscous model was developed. This viscous model was made use of to evaluate the performance of different mitigation measures that were proposed for river levees and other embankments subjected to liquefaction problems.

INTRODUCTION

This paper addresses the prediction of liquefaction-induced deformation of geotechnical structures. A typical example of the deformation is illustrated in Fig. 1 where a building resting on loose sandy deposit tilted and subsided into liquefied subsoil. The significant subsidence and possible tilting were induced by the decrease of soil rigidity under the foundation.

Another important issue is the effect of deformation and displacement on the resistance against large displacement. Fig. 2 demonstrates the empirical knowledge obtained from seismic damage of river levees in Japan for the past over 100 years. It is therein shown that the subsidence of levees, denoted by S, is variable, depending upon the situation, but that S does not exceed 75% of the original levee height, H.

$$S < 0.75\ H \qquad (1)$$

The upper bound of levee subsidence can be understood by considering the equilibrium of weight and buoyancy force. The weight of a levee is governed by the unit weight of compacted soil, which is approximately about 15 kN/m^3 or slightly more, while the buoyancy force that is produced by the liquefied subsoil is produced by the unit weight of saturated sand, which is about 20 kN/m^3. The buoyancy or resistance against subsidence increases as a levee subsides into subsoil. Consequently, as schematically shown in Fig. 3, the force equilibrium is obtained at S = 0.75H that determines the maximum possible displacement.

Fig. 1. Liquefaction-induced subsidence of building during the 1964 Niigata earthquake (Department of Civil Engg, University of Tokyo).

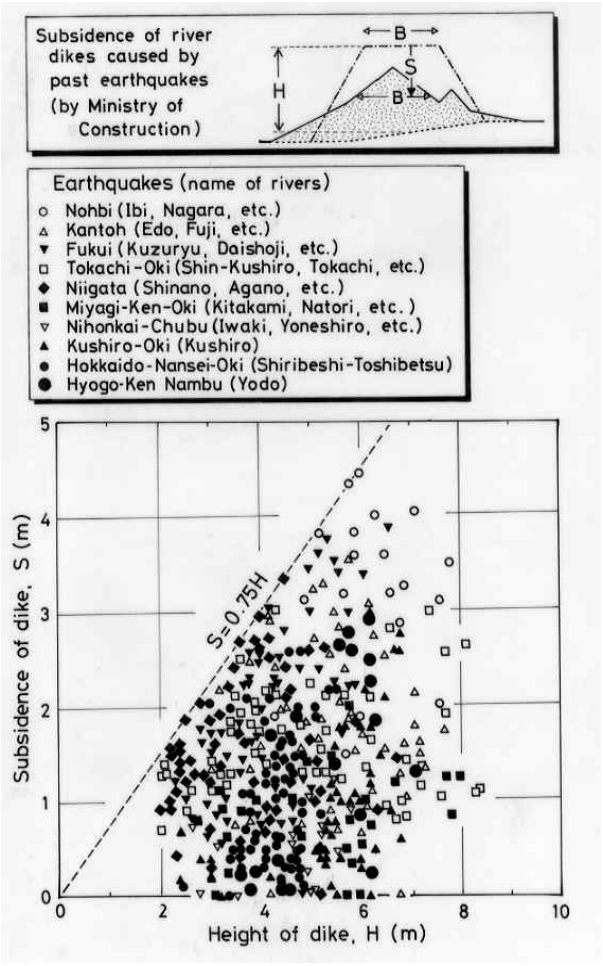

Fig. 2. Empirical relationship between subsidence and height of river levees that underwent earthquake effects.

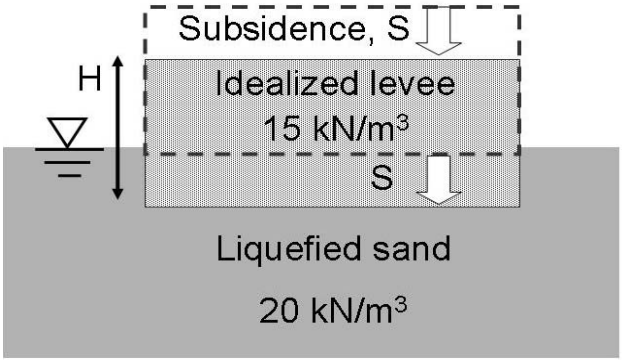

Fig. 3. Maximum possible subsidence of river levee determined by weight-buoyancy equilibrium.

One of the recent trends in geotechnical earthquake engineering is the adoption of performance-based design principle. Although this principle is expected to enable economical design of various structures, it requires soil mechanics to better understand the deformation characteristics of soils that undergo seismic load and to assess the residual deformation that remains after the end of earthquake shaking. In the simplest situation, Newmark [1965] sliding block analogy is able to predict earthquake-induced displacement by using only shear strength of soils. However, liquefaction-induced deformation is out of its scope because liquefied subsoil cannot be considered in any sense a rigid body. In this respect, the present study aims to demonstrate the deformation characteristics of liquefied sand on the basis of experimental results and to apply them to prediction of residual deformation of a geotechnical structure.

PREVIOUS STUDIES ON DEFORMATION CHARACTERISTICS OF LIQUEFIED SAND

Because of its importance in both hazard evaluation and assessment of mitigation measures, experimental studies have been carried out by many people on deformation characteristics of sand that undergoes seismic liquefaction. Since liquefied sand exhibits very soft behaviour, those studies can be classified into two groups that are namely solid-mechanic and fluid approaches.

The solid-mechanic approach employs the traditional soil-mechanic idealization of liquefied sand in which nonlinear stress-strain relationship is focused on. Many elasto-plastic modellings with application to finite element (FE) analyses are of practical interest. Note that most elasto-plastic soil models were developed in 1970s and 80s when large deformation of liquefied ground was not yet interested in, and that those models may not be relevant for the present purposes.

Another solid-mechanic approach comes from an early study by Lee [1974] who conducted cyclic undrained shear of soils and interpreted residual deformation after cyclic loading in terms of reduction of modulus. It was then proposed to run static linear FE analyses twice; the first one with the moduli prior to the cyclic loading and the second with the softened moduli after cyclic shear. The difference of displacement between these two analyses is considered the earthquake-induced distortion. The good point of this method is that modeling of complicated stress-strain behavior of liquefied sand is avoided and replaced by laboratory shear tests, and that it is applicable to both liquefaction and non-liquefaction problems.

Because the above-mentioned Lee's method requires expensive laboratory tests on soil samples, Yasuda et al. [1992] developed a simplified method to determine the extent of modulus reduction by referring to the factor of safety against liquefaction and fines content. Because the two static FE analyses with the initial and the reduced moduli calculate gravity-induced deformation of earth structures, the intensity and duration time of seismic shaking are not explicitly considered in the analysis. They are implicitly considered by the use of the factor of safety against liquefaction. Another important issue is the large-displacement formulation of analysis that is able to account for the variation of buoyancy force with the progress of subsidence (see Fig. 3).

The authors (Towhata et al., 1999) proposed a different approach that is called fluid approach in which liquefied sand is idealized by Newtonian or Bingham viscous liquid. Fig. 4 illustrates early results of 1-G model tests in which an embedded pipe was pulled laterally in liquefied sandy ground. Since the drag force to pull the pipe increased with the pipe velocity, the idea of viscous liquid emerged. This idea thereinafter stimulated discussions which are meaningful from the soil-mechanic viewpoints, and the following chapter is devoted to address their essence so that the significance of the present study may be well understood.

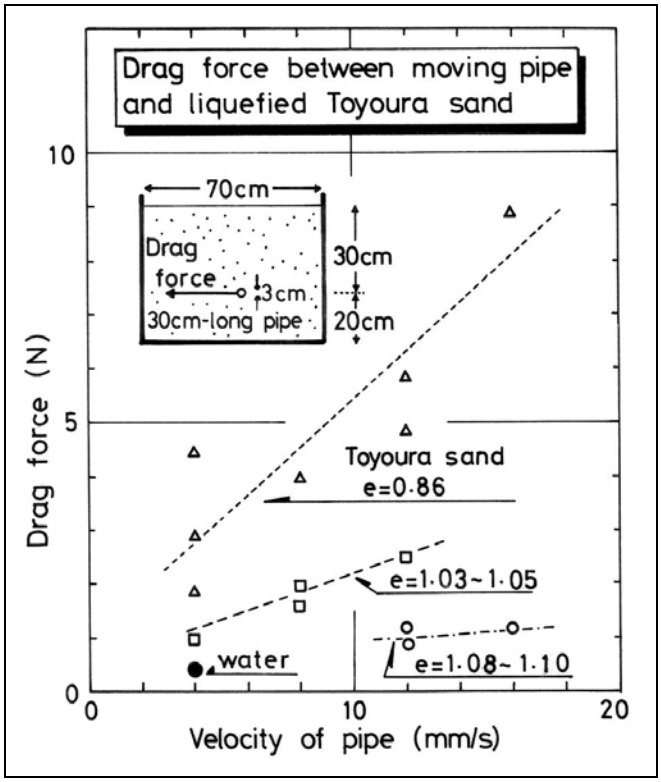

Fig. 4. Positive correlation between drag force and pipe velocity in liquefied model ground.

DISCUSSIONS ON POSITIVE CORRELATION BETWEEN DRAG FORCE AND FLOW VELOCITY

The positive correlation shown in Fig. 4 has been interpreted not in terms of the intrinsic nature of liquefied sand but the pore water pressure difference. As illustrated in Fig. 5 (drawn after model tests by Dungca et al., 2006), possible pore water pressure between front and rear sides of a moving pipe may produce net resistance against motion of the pipe (drag force), and the greater pipe velocity can maintain the greater pressure difference, in spite of seepage, thus leading to rate dependent drag force. Dobry (2007) said that the same mechanism holds true for flow of liquefied sand around a stationary pile foundation. Unfortunately, his discussion was speculative and missed experimental validation.

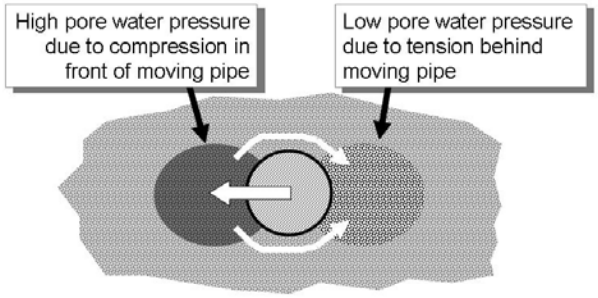

Fig. 5. Pore water pressure difference between front and rear sides of moving pipe that might account for rate dependent drag force.

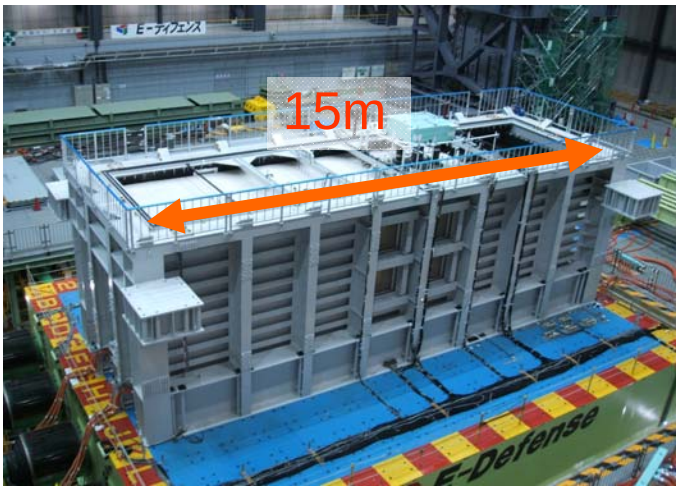

Fig. 6. E-Defense large shaking model test on lateral flow of liquefied sand induced by failure of sheet-pile quay wall.

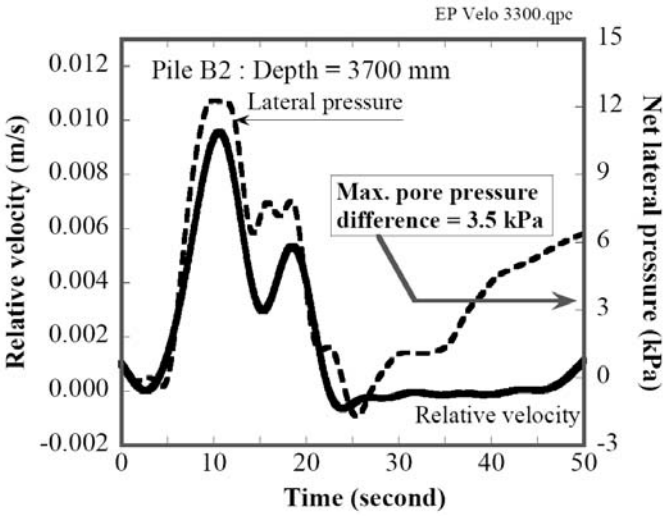

Fig. 7. Variation of lateral pressure on pile model and flow velocity of surrounding liquefied sand (E-Defense test; after Motamed et al., 2009).

The discussion quoted above needs to be carefully examined. First, it does not pay attention to the effective stress and accordingly the total stress, which is the real component of the drag force. Second, during a real earthquake, the pore pressure difference may be erased very quickly around a real pile foundation embedded in pervious sandy subsoil. This issue was examined by using an E-Defense full-scale shaking model test (Towhata, 2008a) on lateral flow of liquefied sand around a pile foundation (Fig. 6). Note that this model test was conducted in a big soil container that measured 15 m in length, 5 m in depth, and 4 m in width, thus generating the stress level equivalent to that in the prototype. The embedded piles were of 15 cm in diameter.

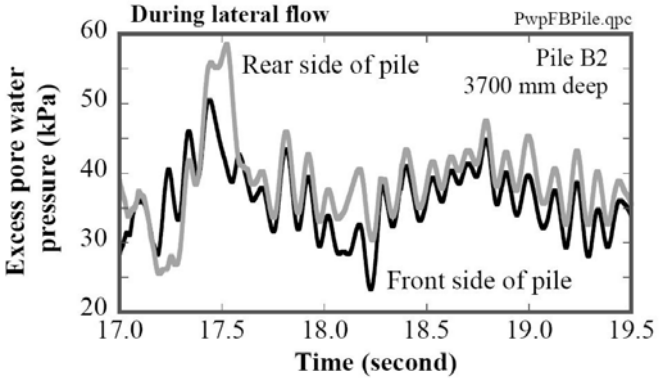

Fig. 8. Time histories of excess pore water pressure in front of and behind a pile subjected to lateral flow of liquefied sand (E-Defense test; after Motamed et al., 2009).

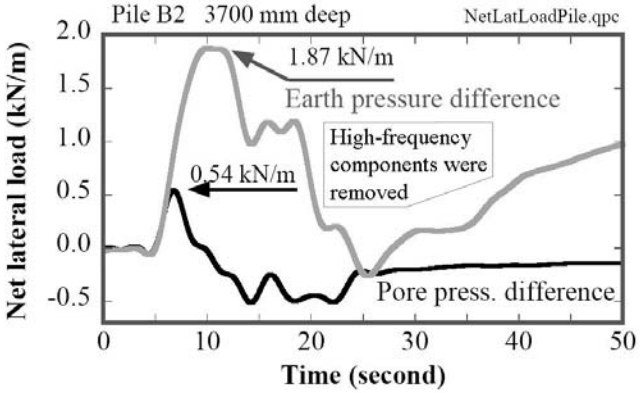

Fig. 9. Comparison of net pore pressure difference and induced lateral load in pile subjected to lateral flow of liquefied subsoil (E-Defense test; after Motamed et al., 2009).

The obtained distortion of the embedded pile foundation behind a tilting quay wall was analyzed in order to demonstrate the deformation characteristics of liquefied sand. Although the analysis was difficult because of the plastic deformation of piles, the elastic part was picked up and examined. First, Fig. 7 illustrates the time histories of lateral earth pressure, which is equivalent to the drag force in Fig. 4, exerted on one of the piles and the relative velocity between flow of surrounding liquefied sand and a pile. The net lateral pressure was obtained by earth pressure transducers installed on two opposite sides of a pile shaft. It is seen in Fig. 7 that there is a good correlation between the net lateral pressure and the change of velocity. This is the same situation as the idea of viscous liquid was originally obtained.

Since the opponent idea of pore pressure difference (Fig. 5) sounds realistic as well, the E-Defense data was further examined in a quantitative manner. Fig. 8 compares the time histories of excess pore water pressure on both the front and rear sides of a pile. It appears in this figure that the pore pressure difference is very small because of the short distance and high permeability of sand. Accordingly, Fig. 9 demonstrates that the net pore pressure difference, which is multiplied by the pile diameter to obtain its contribution per unit length of a pile, is significantly smaller than the lateral load (EP) exerted by the flow of liquefied sand. Thus, the present study quantitatively concludes that, although the theory of pore pressure difference (Fig.5) is interesting, the rate dependency in the lateral earth pressure upon a pile still occurs without the pore pressure difference. Liquefied sand, therefore, has an intrinsically viscous nature.

TRIAXIAL COMPRESSION TESTS IN GRAVITY FIELD

After such model tests as pulling of a pipe and pile bending, their limitation was understood. In those model tests, only force and displacement were directly measured and no information was obtained of the non-uniform states of stress and strain in sand. Hence, it was not possible to obtain the viscous soil parameters of liquefied sand. This limitation is very important in such a material as sand whose mechanical properties are significantly affected by the effective stress level and the magnitude of shear strain.

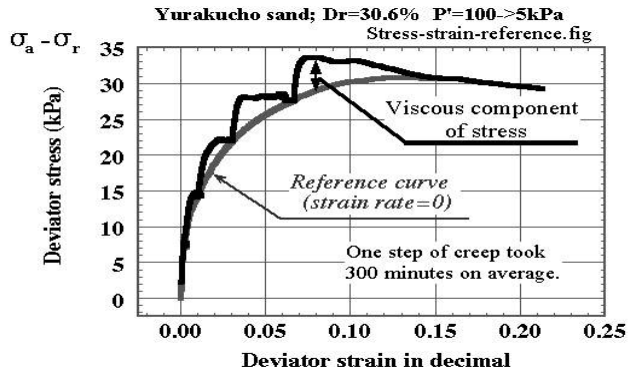

Fig. 10. Stress-strain curve to examine rate-dependent behaviour of sand.

For more reliable measurement of the viscous nature of sand, a series of triaxial compression test was conducted under low effective stress (Gallage et al., 2005, and Towhata, 2008b). Since the research concern therein was the behaviour of liquefied sand, samples of Yuraku-cho sand from Tokyo Downtown were isotropically consolidated under, for example, 100 kPa, and then the confining pressure was unloaded to such a low level as 3 kPa. Samples were then sheared in a triaxial

compression manner and the relationship between the deviator stress and the axial strain was employed for the study of viscous nature of sand under low effective stress.

Figure 10 illustrates how the rate dependent shear stress was obtained from the results of triaxial compression tests. All the tests were conducted with the drainage valve open (drained shear) in order to maintain the pore water pressure constant, thus avoiding the decrease in pore pressure and increase in effective stress as induced by the positive dilatancy under low stress level. In Fig. 10, the axial stress was loaded quickly in several stages, followed by the constant stress. The creep deformation under the constant shear stress was used to determine the shear strain rate. On the other hand, the stress-strain points at the end of creep (zero strain rate) were connected and what is called the reference curve was obtained. This reference curve is of a non-viscous nature (inviscid curve) and its difference from the measured stress-strain curve was considered to be the viscous stress.

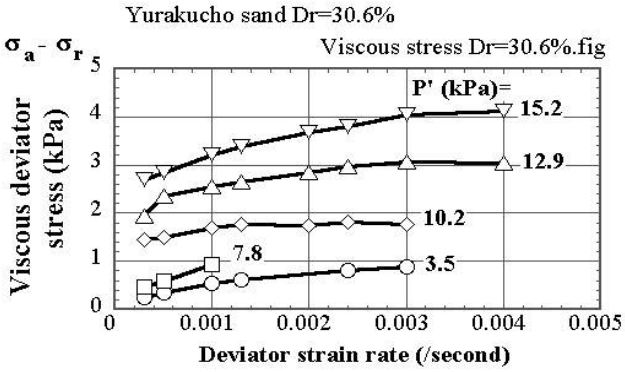

Fig. 11. Variation of rate-dependent component of shear stress with strain rate.

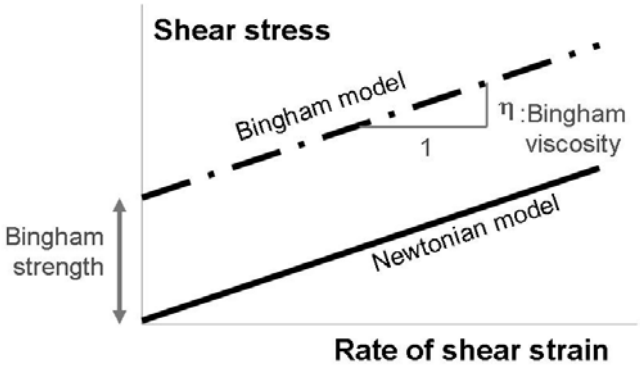

Fig. 12. Conceptual diagram of Bingham viscous model.

Figure 11 exhibits the variation of viscous stress, σ_a-σ_r, with the change of rate of deviator strain. The deviator strain is defined by ε_a-ε_r, which is equivalent with shear strain, γ. Suffices of "a" and "r" stand for the axial and radial components in a triaxial specimen, respectively. Note that the viscous shear stress increased with the increase of the effective mean stress, $P' = (\sigma'_a+2\sigma'_r)/3$, that increases with the loading of axial stress during the triaxial compression. It is important that the viscous stress increases with the strain rate, clearly supporting the idea of Bingham or Newtonian viscous modeling (Fig. 12).

Test results are summarized in Figs. 13 and 14 in which the variation of Bingham viscous parameters are plotted against the effective stress, P'. Data from triaxial extension tests, in which the axial stress was unloaded in order to reduce P', as well as tests on light styrofoam specimens, again for low P', are plotted as well in these figures. It is interesting that the Bingham strength decreases as P' decreases (Fig. 14), and most probably the Bingham strength disappears at zero effective stress, suggesting that liquefied sand with zero effective stress would behave as a Newtonian viscous liquid.

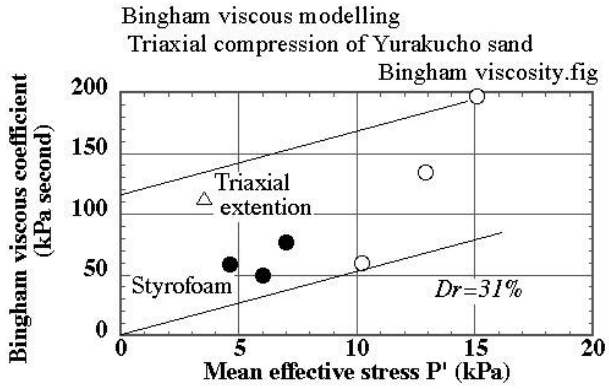

Fig. 13. Variation of Bingham viscous coefficient with effective stress level.

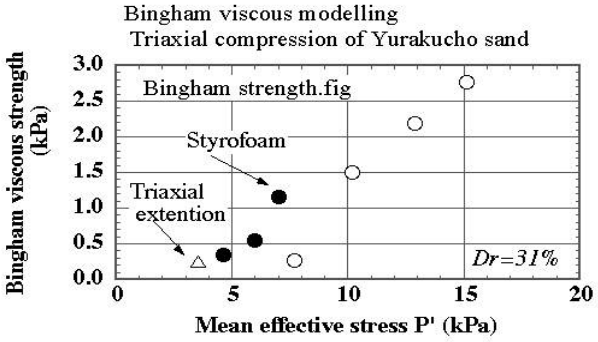

Fig. 14. Variation of Bingham viscous strength with effective stress level.

METHOD OF TRIAXIAL COMPRESSION TESTS IN ZERO GRAVITY ENVIRONMENT

The studies in the preceding chapter revealed a limitation of triaxial compression tests for the experimental study on behaviour of liquefied sand. The problem was that the state of zero effective stress could not be achieved despite that the research aim was the study of liquefied sand with zero effective stress.

Problems under very low stress were;
- Tested specimens become unstable if no confining pressure is applied.
- Because of the weight of soil grains, the axial stresses at the top and the bottom of a specimen are different, and this stress non-uniformity becomes significant if the applied stress level is very low. This heterogeneous stress state in a specimen makes data interpretation very difficult because mechanical behaviour of sand is highly sensitive to the level of effective stress.

To overcome the problems, several ideas were examined. For example, however, the use of a light material, such as Styrofoam in Fig. 13, still could not achieve zero confining stress. Also the idea of heavy liquid in which the buoyancy force could cancel the gravity force could not find suitable liquid, some being too heavy and others too light, and most of them being poisonous and hazardous. Consequently, the idea of triaxial compression tests in a zero-gravity environment was obtained.

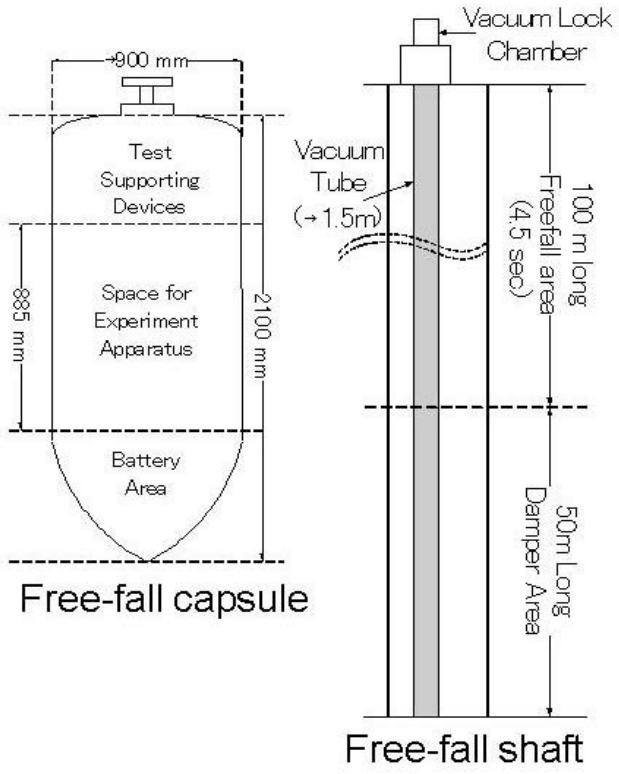

Fig. 15. Underground vertical shaft for free fall test at MGLAB.

Sture et al. [1998] carried out triaxial compression tests in a NASA Space Shuttle in which gravity was negligible. This kind of test is extremely expensive and, to the authors' speculation, the inertial effect upon lift-off of a shuttle makes the sand specimen overconsolidated. A second idea for zero gravity tests is the use of an aircraft that flies freely without engine propulsion. This idea is again expensive and also tests aboard a plane do not allow sufficient time for sample preparation. Thus, finally, the idea of free-fall tests was adopted.

Free-fall tests were carried out at MG (Micro Gravity) Laboratory in Toki, Gifu, Japan. Figure 15 presents the general idea of the facility; testing device is installed in a free-fall capsule, the capsule is placed at the top of a vertical shaft, air in the entire shaft is removed, keeping the atmospheric pressure inside the capsule, and the capsule falls freely over 100 m. After this free fall, the damper at the bottom stops the capsule, and then the acceleration could be as large as 10 times gravity. Fig. 16 illustrates the size of a freefall capsule in which a triaxial device is encased. This figure shows sample preparation going on.

A triaxial compression device was newly designed and fabricated for the free-fall tests. The basic requirement for the device concerned
- small size because of the limited space in the capsule (Fig. 16),
- light weight that reduces the impact force small upon landing at the bottom of the free-fall shaft (Fig. 15),
- safety requirement, avoiding the use of pressurized air, and
- remote control of pore pressure and axial loading during free fall from outside through wireless communication.

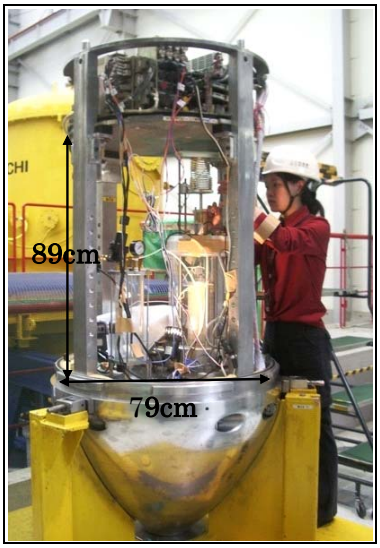

Fig. 16. Free-fall capsule that encases triaxial testing device.

These requirements were satisfied by the design in Fig. 17 in which major points are as what follows.
- The confining pressure was supplied not by the external pressurized air but by negative back pressure inside a specimen. The negative pressure was supplied from a vacuum tank through a regulator. Thus, the risk of explosion of the pressurized chamber was avoided.
- To reduce the weight, the axial stress was loaded by a simple spring system. The natural length of the spring was set long enough so that its minor deformation upon 10 or 20 % axial strain of the sample might not cause significant change in the axial load.

- Electronic cramps and valves were installed and controlled through wireless from outside in order to accurately control the time of releasing the negative back pressure (making the effective stress zero) and the time of starting axial compression.

All data was recorded in a logger aboard the capsule.

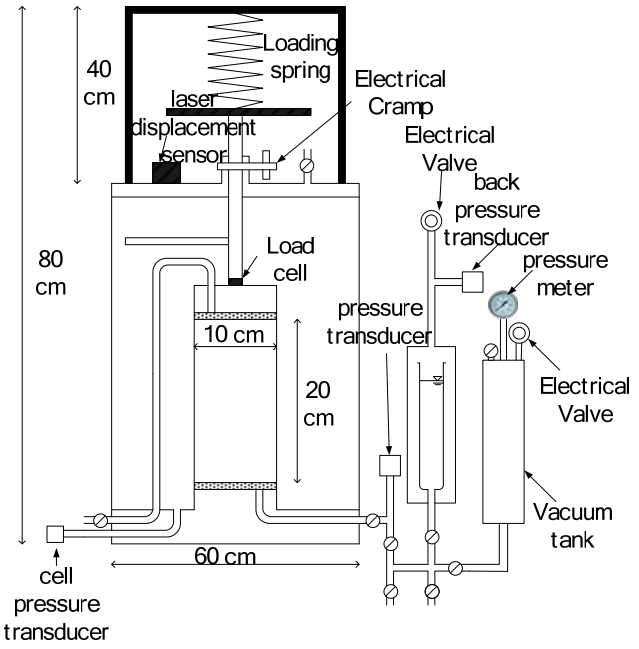

Fig. 17. Triaxial shear device designed for free fall tests.

Fig. 18. Free fall capsule at the top of vertical shaft.

The sequence of a test is summarized in what follows.

(1) A Toyoura-sand specimen was prepared in a sample preparation room by using the air-pluviation technique in 1-G field with the target relative density of around 50 %. The sample size was 20 cm in height and 10 cm in diameter. De-aired distilled water was circulated through the sample so that Skempton's *B* value might be greater than 0.95. Later, however, the use of water-saturated specimens was replaced by that of dry sand, as will be discussed later.

(2) The specimen was isotropically consolidated under 100 kPa by applying air confining pressure as conducted in regular procedure of triaxial tests.

(3) Spring mechanism for axial stress was compressed but locked so that no effect would occur prior to free fall.

(4) The confining pressure was reduced to 20 kPa that is generated by negative pore pressure. Thus, the air confining pressure as mentioned in (1) was released to null. The triaxial device was placed in a capsule and transported to the top of the vertical shaft (Fig. 18).

(5) Immediately after the beginning of free fall through a vacuumed shaft, the negative back pressure was released to generate the state of very low effective stress. The stress history thus conducted intends to reproduce what happens in real liquefaction where sand is initially consolidated by the overburden and the stress level then decreases to null due to excess pore water pressure during shaking.

(6) Then, the locking of the spring was released quickly and the deviator stress was loaded. The induced creep deformation was measured and recorded. The state of zero gravity lasted for approximately 4 to 5 seconds. The viscosity coefficient was obtained by dividing the shear stress, $(\sigma_a - \sigma_r)/2$, by shear strain rate, $d(\varepsilon_a - \varepsilon_r)/dt$, where ε_a stands for the axial strain and ε_r the radial strain that is approximately given by $-\varepsilon_a/2$.

It is noteworthy that the drainage valve was kept open during the creep because pore pressure had to be maintained unchanged and effective stress at very low level by preventing decrease of pore pressure caused by positive dilatancy. This idea is identical with what was employed in the aforementioned triaxial tests in 1-G field.

Special care was taken of data interpretation to account for the effects of acceleration and related inertia force on stress. That is, the mass of the vertical loading shaft, the loading platen, and sand grains was multiplied by the acceleration of the falling device minus the exact gravity acceleration and this minor axial load was added to the spring force to precisely calculate the axial stress. Additional correction was made of the membrane tensile force that affected the radial confining stress. Finally, the axial stress was calculated by considering the change of the sample's cross section by assuming that the radial strain is equal to half of the axial strain ($-\varepsilon_a/2$).

The first free-fall test was thus prepared and conducted in May, 2007. This test, however, was not successful and no creep deformation occurred. The reason for this is presented in Fig. 19, where the negative pore water pressure could not come back to zero as initially planned. This problem occurred because the back pressure channels were made of slender pipes and, although this size was reasonable for conventional triaxial tests, they were too small to supply the external atmospheric pressure quickly enough to cancel the internally generated negative pore water pressure due to positive dilatancy of sand under very low effective stress. Therefore, it was decided to run

the following free-fall tests on dry samples for which external air pressure was transmitted quickly through the slender channel and the negative air pressure was cancelled successfully.

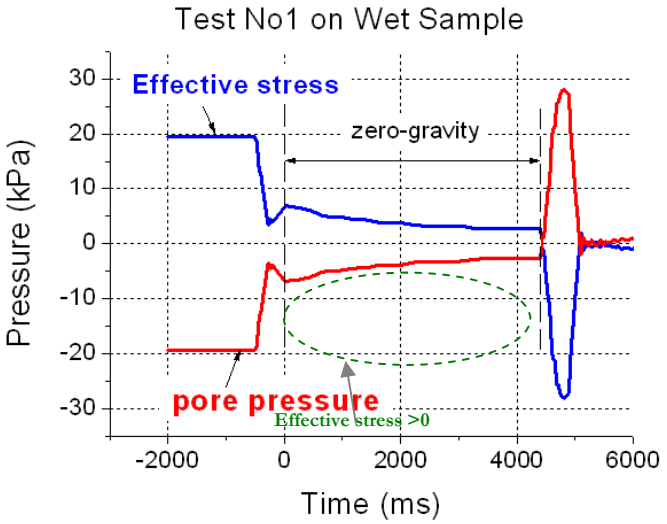

Fig. 19. Change of pore pressure during unsuccessful free fall test on water-saturated specimen.

RESULTS OF MICRO-GRAVITY TRIAXIAL COMPRESSION TESTS ON DRY SPECIMENS

Two free-fall tests were run successfully on air-dry sand samples. The appearances of a tested specimen (Test 4) in the course of free-fall creep deformation and after collapse upon landing the bottom of the shaft are shown in Fig. 20.

Figure 21 indicates the time history of axial strain for a sample of 53 % relative density. Note that no stress history of 100 kPa consolidation was practiced in what follows prior to the free fall. The confining pressure (σ'_3) was as low as 0.6 kPa. The time change of axial strain in Fig. 21 consists of two phases, which are the first quick increase at 0.6 second, that was caused by the releasing the lock of the axial load, and the following creep distortion after 1.5 second. The rate of axial strain was approximately 0.01 /s (1 %/s). This constant rate of stress indicates that creep deformation occurred without acceleration due to mass or gravity effects.

The stress-strain behavior in this test is shown in Fig. 22. The deviator stress was raised up to nearly 11 kPa. Note that the creep deformation in Fig. 21 occurred after the deviator stress achieved this peak value. The minor decrease of the deviator stress after the peak state was caused by the increase of the cross section of the specimen. It is interesting that the peak deviator stress together with the low confining pressure suggests the friction angle to be as high as 65 degrees. It should be recalled now that Sture et al. [1998] carried out triaxial shear on dense sand under 0.05 to 1.30 kPa and reported the friction angle to be as high as 70 degrees.

(a) During creep (b) After landing and impact

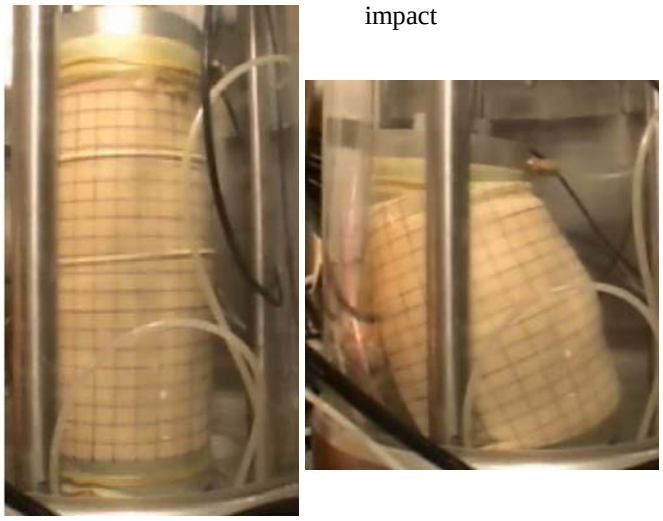

Fig. 20. Appearance of specimen during and after free fall (Test 4).

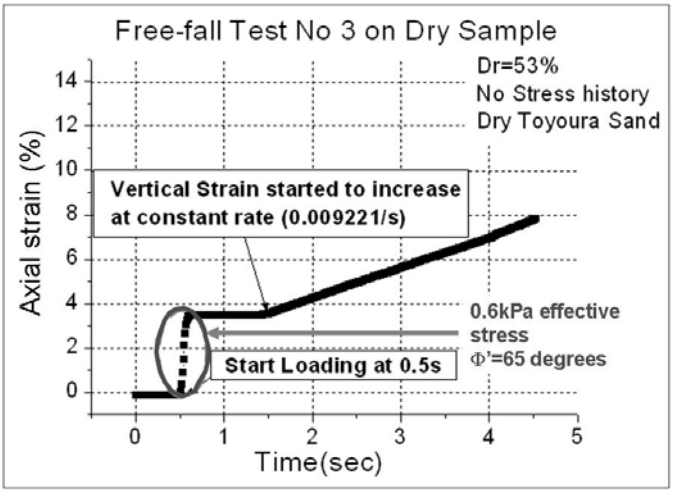

Fig. 21. Time history of axial strain of dry specimen during free fall (Test No. 3).

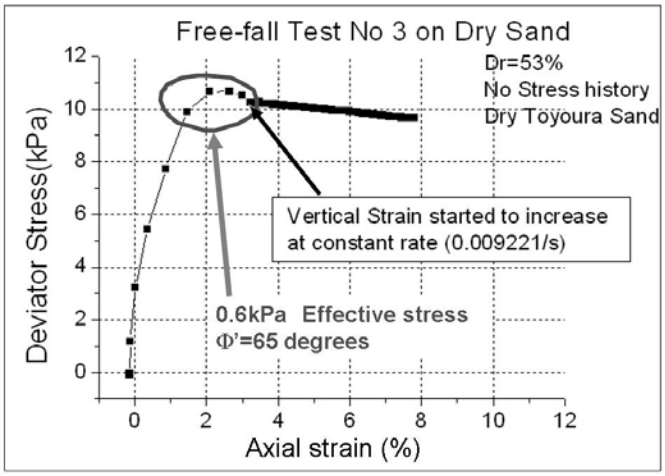

Fig. 22. Stress-strain behavior of dry sand during free fall test No.3.

The second free-fall test was conducted on a looser specimen with its relative density being 36 %. The results in Fig. 23 show that the confining pressure was 0.28 kPa and the peak deviatoric stress was nearly 11 kPa, thus making the friction angle 71 degrees. Note that this looser specimen achieved the peak stress at a greater strain than the denser specimen in Fig. 22. The results of free fall tests were substituted in the following formula in order to calculate the shear viscosity coefficient. Note that this formula assumes the Newtonian viscosity and the Bingham strength (Fig. 12) is ruled out because the effective stress is very low.

$$\text{Viscosity coefficient} = \frac{(\sigma_1-\sigma_3)/2}{\frac{d}{dt}(\varepsilon_a-\varepsilon_r)} = \frac{(\sigma_1-\sigma_3)/2}{\frac{d}{dt}(\varepsilon_a \times 1.5)} \quad (2)$$

Note that the radial strain is herein assumed to be half of the axial strain.

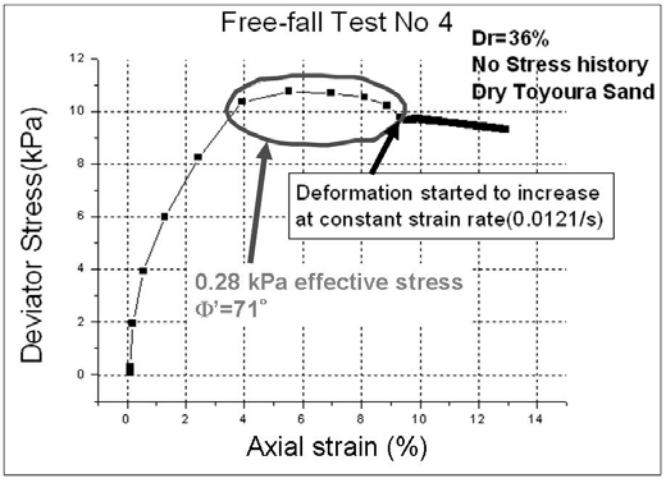

Fig. 23. Stress-strain behavior of dry sand during free fall test No.4.

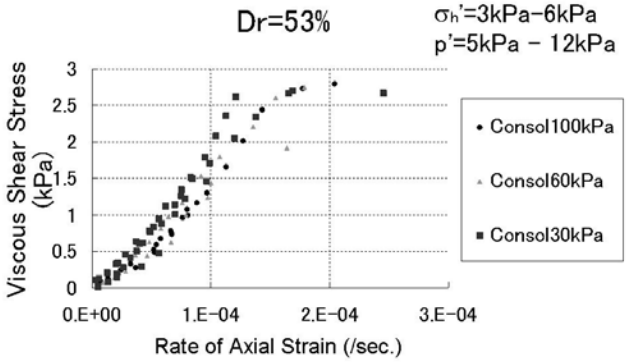

Fig. 24. Relationship between viscous stress and strain rate under low effective stress and normal gravity conditions (relative density = 53%).

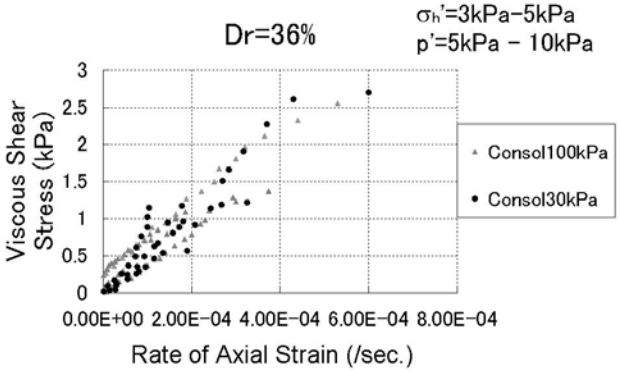

Fig. 25. Relationship between viscous stress and strain rate under low effective stress and normal gravity conditions (relative density = 36%).

SUPPLEMENTARY TRIAXIAL COMPRESSION TESTS IN 1-G FIELD

Since the number of free-fall tests was limited because of the schedule of the facility, additional tests were run in 1-G field using the same triaxial device. Although the stress level (P' = 5 to 10 or 12 kPa) was not so low as that in the free fall tests, still meaningful information was obtained and utilized in comparison with the free-fall data. The viscous stress was determined by using the method in Fig. 10.

Figure 24 demonstrates the variation of viscous shear stress with the rate of axial strain. The relative density of sand was around 53 % and the confining pressure was in the range of 3 to 6 kPa. While samples were consolidated initially under three different pressures (30, 60, and 100 kPa), there is not a significant difference in the measured viscous stress. Similar finding is made in Fig. 25 in which the sand was looser (36% relative density).

DISCUSSION ON VISCOSITY OF LIQUEFIED SAND

The viscous or rate-dependent nature of sand that have been so far obtained from free-fall and 1-G tests are assembled in Fig. 26 by using the viscous shear stress, $(\sigma_a-\sigma_\rho)/2$, and the axial strain rate, $d\varepsilon_a/dt$. This figure indicates that denser sand has greater viscosity than looser sand in 1-G tests whilst the effect of density is not clear in free-fall tests (Figs. 22 and 23). It is evident further that viscosity coefficient, η, that is obtained by the ratio of viscous shear stress and strain rate, substantially changes with the magnitude of strain rate. This nonlinearity implies that a practical value of viscosity coefficient can be obtained after determining a realistic value of strain rate. This goal is tentatively achieved by referring to the subsidence of Niigata Airport Building during the 1964 Niigata earthquake. There is no other information from real liquefaction phenomenon by which the rate of strain is determined.

A motion picture of on-going liquefaction and subsidence of

the terminal building in Niigata Airport was taken by a professional photographer, Mr. Fukuo Yuminamochi, who was in the airport building at the moment when the earthquake motion started. His motion picture is now available from the Japanese Geotechnical Society.

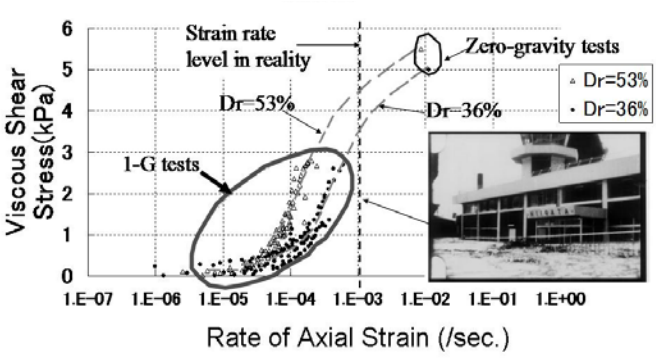

Fig. 26. Relationship between viscous shear stress and axial strain rate under low effective stress and normal gravity conditions.

Fig. 27. Boiled water around Niigata Airport (air photograph taken by Mr. Yuminamochi immediately after the quake).

Fig. 28. Subsided shape of Niigata Airport Terminal Building (Department of Civil Engineering, University of Tokyo).

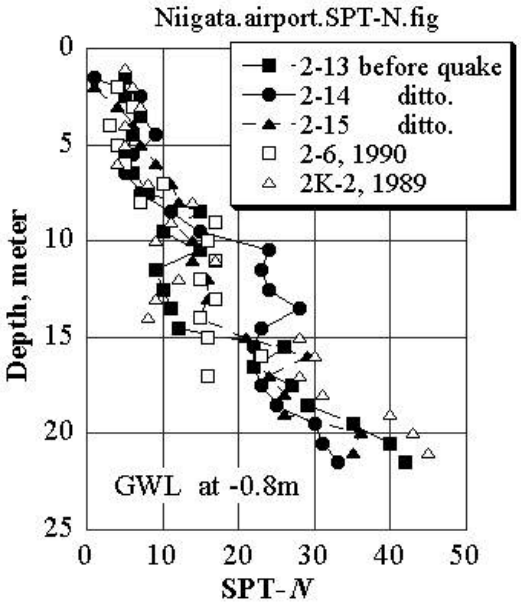

Fig. 29. SPT profile in foundation of Niigata Airport building (data by Ministry of Transport and Kiso-Jiban Consultants Company).

In Niigata Airport, subsoil liquefaction occurred dramatically around the building and the ground surface was covered by boiled water (Fig. 27). Consequently, the building subsided more than one meter, but no structural damage occurred, implying that shaking was weakened by liquefaction (Fig. 28). The first author examined the motion picture and evaluated the rate of building subsidence to be around 1 cm/s (Towhata and Horikoshi, 1997). In addition, the thickness of liquefied sand is assessed by referring to the SPT-N profile in Fig. 29. Although the exact number cannot be obtained because of the information lack of surface ground motion, the thickness of liquefaction was most probably between 7 m and 13 m. By using the rate of subsidence of 1 cm/s, it is reasonable to say that the rate of axial (vertical) strain was 1cm/s / 10m = 0.001 /s. This strain rate is shown in Fig. 26 and Eq. 2 gives the viscosity to be η = 2,700 kPa.Second.

ANALYSIS ON LIQUEFACTION-INDUCED GROUND DEFORMATION BY USING VISCOUS MODELLING

Towhata et al [1999] developed a computer code that calculates the time history of liquefaction-induced ground deformation in a two-dimensional manner. This method of analysis makes use of the aforementioned viscous modeling of liquefied sand as well as the principle of minimum potential energy and the theory of Lagrangean equation of motion. This computer code is now available free of charge from Japan Institute of Construction Engineering under the name of SOLIFLUK (SOiL In FLow Under Kinematics). Kobayashi and Towhata (2009) further developed this analysis by considering more general modes of deformation in a three-dimensional manner.

The present study employed this developed version of analysis to reproduce the subsidence of Niigata Airport Building. Two values of the thickness of liquefaction were employed and the viscosity coefficient was set equal to 2,700 kPa.Sec,

The calculated time history of subsidence is shown in Fig. 30. It is interesting that calculated and real rate of subsidence for 2,700 kPa.Sec viscosity are consistent, irrespective of the uncertain thickness of liquefaction. Note that the end of subsidence is set at the end of strong shaking. Interpretation of past strong earthquake motions (Fig. 31) gives an empirical correlation between the duration time of strong shaking (more precisely the time between the peak acceleration and the end of shaking stronger than 50 cm/s^2) and the earthquake magnitude. Since the 1964 Niigata earthquake was of 7.5 magnitude, the duration time of ground deformation is more or less 40 to 50 seconds. This idea of duration time of strong shaking and subsoil flow is not consistent in Fig. 30 with the ultimate building subsidence of 1.2m. It seems therefore that ground flow lasted for a longer time.

The viscosity coefficient thus validated was employed for performance assessment of measures that can mitigate the liquefaction-induced deformation of geotechnical structures. Fig. 32 exhibits a cross section of an imaginary embankment resting upon a liquefiable substrata. Material properties are presented in this figure. Note that the Young modulus, E, of the surface unliquefiable soil is made null if tensile deformation is calculated. This idea is consistent with the fact that river levees developed tensile cracks upon their lateral spread (Fig. 33).

The first run of analysis was conducted on the cross section in Fig. 32 that has no mitigation measure. Fig. 34 illustrates the elevation difference after 20 seconds of viscous flow under the action of gravity. This duration time is equivalent to the earthquake magnitude of 7 in Fig. 31. The subsidence of 1.04 m at the crest induced the 9.5-cm uplift of the bottom. Note that the present analysis assumes a constant-volume (undrained) deformation of soil, subsidence is compensated for by uplift elsewhere. To take into consideration the consolidation settlement, the thickness of liquefied layer is multiplied by the probable volumetric strain (typically 3% in loose sand) and this subsidence is superimposed on Fig. 34.

Time history of subsidence at crest is plotted in Fig. 35, while Fig. 36 shows the development of lateral displacement at the toe of the slope. When the earthquake magnitude is greater, the duration time of flow deformation becomes longer and accordingly the displacement increases as well.

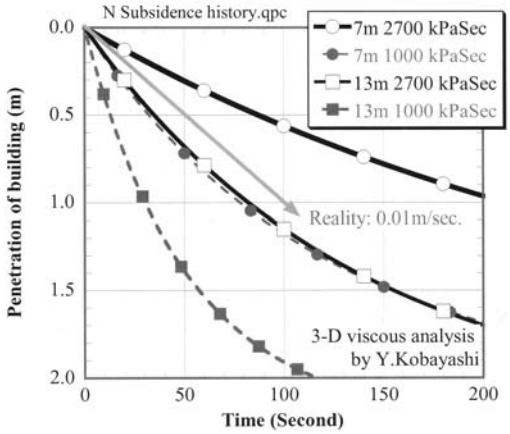

Fig. 30. Subsidence of Niigata Airport Building as calculated by three-dimensional viscous-liquid analysis.

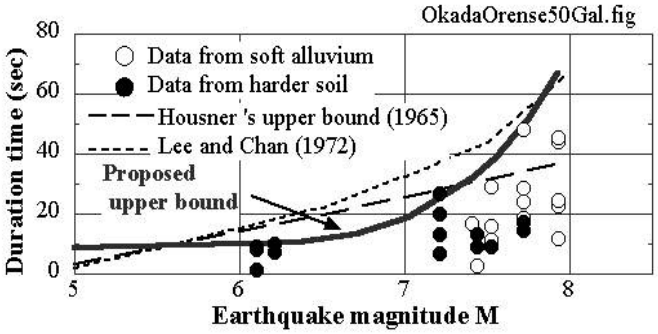

Fig. 31. Duration of acceleration stronger than 50 Gal after maximum acceleration (Okada et al., 1999).

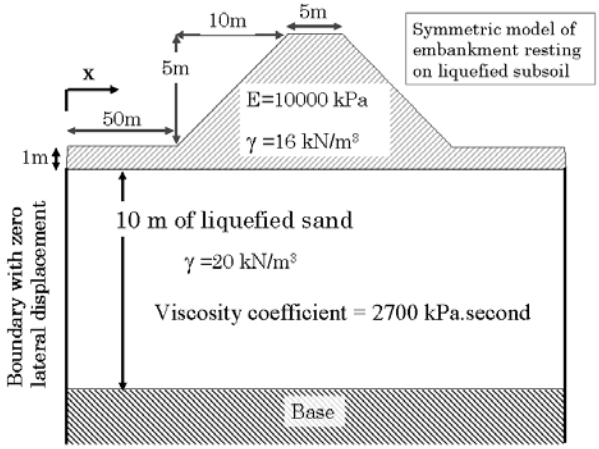

Fig. 32. Model of embankment subjected to liquefaction-induced subsidence and lateral spread.

Fig. 33. Longitudinal cracks along river dike (Ushi-shubetsu River after 2003 Tokachi-oki earthquake).

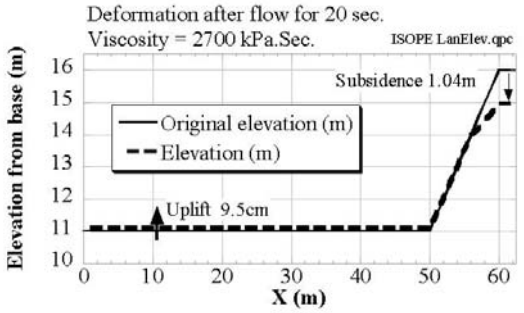

Fig. 34. Change of surface elevation after 20 seconds of deformation.

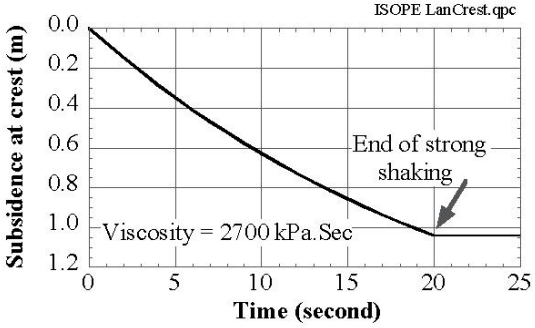

Fig. 35. Time history of subsidence at crest of embankment.

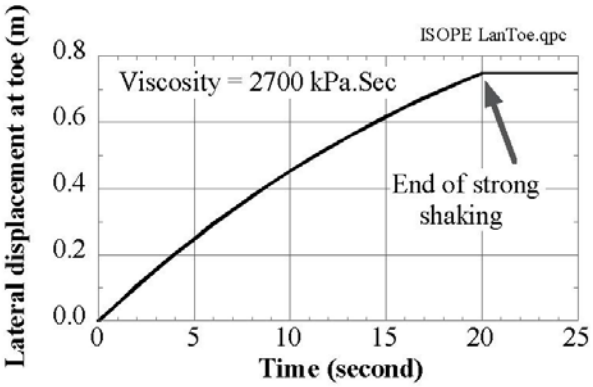

Fig. 36. Time history of lateral spread at toe of embankment slope.

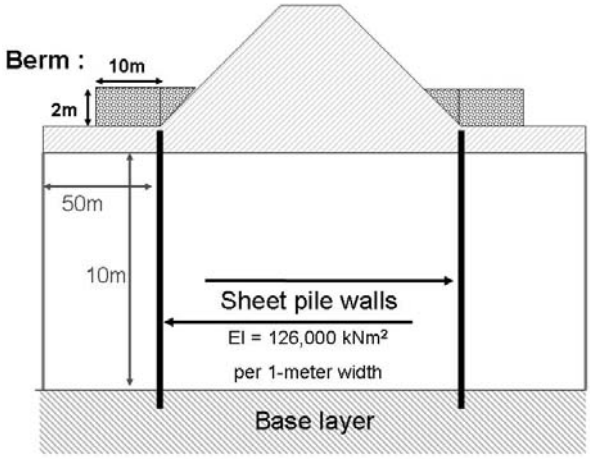

Fig. 37. Mitigation of liquefaction-induced subsidence of embankment by berms or sheet pile walls at the toe of slopes.

For the assessment of their effects, two mitigation measures and their combination were investigated. The first of them is a soil berm. In the present study a berm of 2 m in height and 10 m in width was placed at both toes of the embankment slope (Fig. 37). The effects of the berm are expressed as the over-burden pressure of 32 kN/m^2 in the present study; this counter-weight being able to improve the stability of the slope. The second mitigation is the installation of sheet-pile walls below the toes of the slopes (Fig. 37) whose flexural rigidity is EI = 126,000 kNm^2 per 1-meter width of the wall (Sheet pile of Type 5) and whose bottom is fixed without rotation in an unliquefiable base soil. Finally, the combination of these two measures were examined.

The calculated time history of crest subsidence is plotted in Fig. 38 for all the three mitigation choices together with the one without mitigation (Fig. 35). It is found here that the use of sheet pile or its combination with a counter-weight berm is useful.

In practice, sheet piles have been installed under slope toes of river levees. Those sheet piles have not been intended to mitigate the liquefaction problems but to reduce the seepage flow of river water under a levee when flooding raises the river water level. Since the mechanical stability has not been the aim of those piles, the bottom of the sheet pile is not always embedded in the stable base layer. In this respect, further analyses were conducted by varying the length of sheet pile walls as shown below.

- No sheet pile wall is installed.
- Sheet pile is only 5 m long and covers only the upper half of the liquefiable layer. Its top is fixed; no rotation and translation with the surface soil, and the bottom is floating in liquefied sand, being free to rotate.
- Sheet pile wall reaches the bottom of the liquefied layer; its length being 10 m. However, the bottom is not fixed but

free to rotate and translate laterally. The upper boundary condition is identical with what was stated above (fixed end).
- Same kind of sheet pile as analyzed in Fig. 37; both top and bottom being fixed.

For details of calculation, refer to Towhata [2009].

Variation of crest subsidence after 20 second flow is indicated in Fig. 39 for three kinds of sheet pile length. Insufficient length of piles does not improve the crest subsidence. Thus, the fixed boundary condition at the bottom is extremely important.

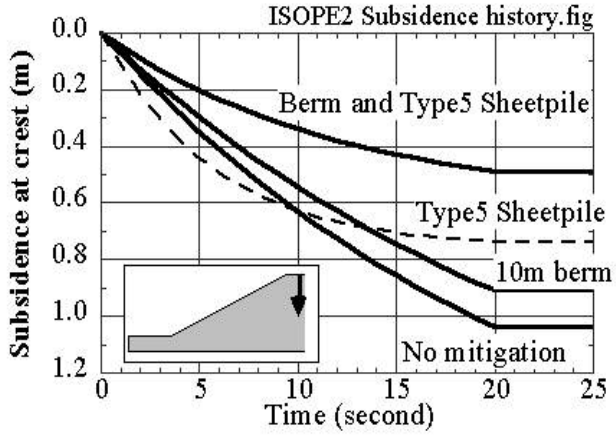

Fig. 38. Effects of two mitigation measures on subsidence of crest of embankment underlying liquefiable subsoil.

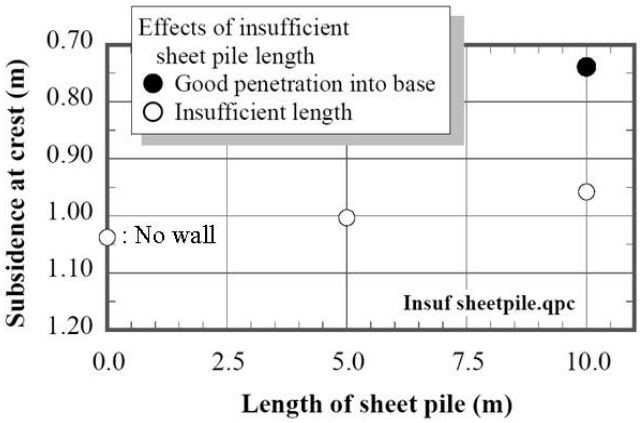

Fig. 39. Effects of insufficient length of sheet pile walls on magnitude of crest subsidence.

CONCLUSIONS

The present study investigated the deformation characteristics of liquefied sand undergoing very low effective stress. Although early model tests suggested rate-dependent or viscous nature of liquefied sand, the non-uniformity of stress and strain in the model ground made it difficult to examine the stress and strain states. Accordingly, the authors carried out triaxial compression tests in which the extremely low effective stress was produced by free-falling tests where the gravity effects disappeared. Major conclusions drawn from this study are as what follows.

1) Liquefied sand behaves like viscous liquid.
2) The viscosity coefficient of sand exhibits significant nonlinearity in which the coefficient varies with the change of shear strain rate.
3) The strain rate and viscosity coefficient that are relevant for practical calculation were determined with referring to a case history during the 1964 Niigata earthquake.
4) The obtained viscosity coefficient was utilized in numerical analyses in which the liquefaction induced deformation of geotechnical structures was assessed and the effects of mitigative measures were assessed.

ACKNOWLEDGMENT

The present study was supported by the financial granted Ministry of Education, Culture, Sports, Science and Technology. The free-fall tests were conducted with the assistance of Mr. M. Nokura at Micro-Gravity Laboratory of Japan, Toki, Japan. Performance tests of a developed free-fall triaxial device were helped by Prof. Tsue, Department of Aeronautics and Astronautics, University of Tokyo. Data obtained by the full-scale shaking table test at E-Defense was very valuable. These supports are deeply appreciated by the authors.

REFERENCES

Dobry, R. [2007]. Discussion, 4th Int. Conf. Earthq. Geotech. Engg., Thessaloniki.

Dungca, J. R., J. Kuwano, A. Takahashi, T. Saruwatari, J. Izawa, H. Suzuki and K. Tokimatsu [2006]. “Shaking Table Tests on the Lateral Response of a Pile Buried in Liquefied Sand”, Soil Dynam. Earthq. Engg., Vol. 26, pp. 287-295.

Gallage, Chaminda P.K., I. Towhata, and S. Nishimura [2005]. "Laboratory Investigation on Rate-dependent Properties of Sand Undergoing Low Confining Effective Stress”, Soil. Found., Vol. 45, No. 4, pp. 43-60.

Kobayashi, Y. and I. Towhata [2009]. “Three Dimensional analysis of Ground Deformation Caused by Seismic Liquefaction”, to be submitted to Soil. Found.

Lee, K.L. [1974]. “Seismic Permanent Deformation in Earth Dams”, Report to NSF, No. GI38521.

Motamed, R., I. Towhata., T. Honda, S. Yasuda, K. Tabata, and H. Nakazawa. [2009]. “Behaviour of Pile Group behind a Sheet Pile Quay Wall Subjected to Liquefaction-induced Large Ground Deformation Observed in Shaking Test in E-

defense Project, Soil. Found., Vol. 49, No. 3, pp. 459-475.
Newmark, N.M. [1965]. “Effects of Earthquakes on Dams and Embankments”, Geotech., Vol. 5, No. 2, pp. 137-160.

Okada, S., R.P. Orense, Y. Kasahara, and I. Towhata [1999]. “Prediction of Liquefaction-induced Deformations of River Embankments”, Proc. 2nd Int. Conf. Earthq. Geotech. Engg., Vol. 2, pp. 543-548.

Sture, S., N. Costes, S. Batiste, M. Lankton, K. Alshibli, B. Jeremic, R. Swanson, and M. Frank [1998]. “Mechanics of Granular Materials under Low Effective Stresses”, Journal of Aerospace Engineering, ASCE, Vol. 11, No. 3, pp. 67-72.

Towhata, I., W. Vargas-Monge, R.P. Orense, and M. Yao [1999]. “Shaking Table Tests on Subgrade Reaction of Pipe Embedded in Sandy Liquefied Subsoil”, Soil Dynam. Earthq. Engg., Vol. 18, No. 5, pp. 347-361.

Towhata, I., R.P. Orense and H. Toyota [1999]. "Mathematical Principles in Prediction of Lateral Ground Displacement Induced by Seismic Liquefaction", Soil. Found., Vol. 39, No. 2, pp. 1-19.

Towhata, I. and K. Horikoshi [1997]. “Case History Study on Liquefaction-induced Subsidence of Niigata Airport Building”, Proc. 32nd Ann. Conv. Japan. Geotech. Soc., Vol. 1, pp. 973-974 (in Japanese).

Towhata, I. [2008a]. Geotechnical Earthquake Engineering, Springer, p. 528.

Towhata, I. [2008b]. Ditto, pp. 566-567.

Towhata, I. [2009]. “User’s Manual for SOLIFLUK Analysis for Flow Deformation of Liquefied Ground”, Japan Inst. Construction Engg., Tokyo (in Japanese).

Yasuda, S., H. Nagase, H. Kiku, and Y. Uchida [1992]. The Mechanism and a Simplified Procedure for the Analysis of Permanent Ground Displacement due to Liquefaction”. Soil. Found., Vol. 32, No. 1, pp. 149-160.